Materials Science Forum
ISSN: 1662-9752, Vol. 1014, pp 14-21
doi:10.4028/www.scientific.net/MSF.1014.14

Submitted: 2020-06-24
Revised: 2020-08-31
Accepted: 2020-09-01
Online: 2020-11-16

High Temperature Annealing SP-AlN Ameliorates the Crystal Quality of $Al_{0.5}Ga_{0.5}N$ Regrowth

Wenkai Yue[1,a], Zhimin Li[2], Xiaowei Zhou[1], Jinxing Wu[1], Yanli Wang[1], and Peixian Li[1,b]

[1]State Key Discipline Laboratory of Wide Band Gap Semiconductor Technology, Xidian University, Xi'an 710071, China

[2]School of Advanced Materials and Nanotechnology, Xidian University, Xi'an 710071, China

[a]wkyue@stu.xidian.edu.cn, [b]pxli@mail.xidian.edu.cn.

Keywords: Crystal morphology, Nitrides, Semiconducting aluminium compounds

Abstract. In this study, the effect of a high-temperature annealing process on AlN is investigated. The high-temperature annealing process reduces the screw dislocation density of the AlN film to $2.1 \times 10^7 \mathrm{cm}^{-2}$. The AlN surface is highly flat. Through HRXRD , the stress mode changes in the sputtered AlN film before and after high-temperature annealing were studied in depth. Based on the HTA-AlN template, a high-quality, high-Al composition AlGaN epitaxial wafer, with a (0002) plane rocking curve FWHM of 246 arcsec , was prepared at 1080°C The growth mode of AlGaN grown directly on the AlN template at low temperature is summarized.

Introduction

In recent years, deep ultraviolet optoelectronic devices based on AlGaN with high Al composition have attracted much attention due to their wide application in sterilization and disinfection, solar blind detection, high-density optical data storage systems, and biomedicine [1, 2, 3, 4]. Due to the limitations of the massive AlN substrates and the small size of AlN wafers, the AlN and AlGaN layers of most deep ultraviolet devices are now fabricated on sapphire substrates; these substrates are transparent to ultraviolet light heterogeneous epitaxial growth [5, 6]. However, there are many disadvantages with respect to epitaxial AlN growth on sapphire substrates. For example, Al atoms need to overcome a large migration barrier on the sapphire surface; there is a large lattice mismatch and thermal mismatch between the AlN materials and sapphire substrate. Both of these factors lead to the poor quality of the AlN epitaxial layer grown on sapphire and the high dislocation density of the epitaxial layer [7].

Many methods have been proposed to improve the quality of heteroepitaxial AlN layers on sapphire substrates, including molecular beam epitaxy [8], nanopattern etching on sapphire substrates [9], migration-enhanced metal organic chemical meteorological deposition technology [10], high-temperature MOCVD [11] and pulsed laser deposition [12]. Additionally, for the purpose of achieving low TDD, the effect of increasing the mutual dislocation and extinction with increasing thickness of the AlN layer can be used. The thicker the AlN layer is, the higher the chance is for climbing dislocations with opposite Burgers vectors meeting each other and disappearing. This effect requires a layer thickness of a few microns. Therefore, a method must be found to reduce the tensile stress that may cause cracking after only a few hundred nanometers of continuous, smooth AlN growth.

Until recently, high-temperature (HT) annealing technology for sputtering AlN has been utilized. The traditional physical sputtering method for growing AlN typically uses a lower sputtering temperature, so the sputtered AlN film usually shows poor crystallinity. The research of Miyake et al. shows that when post annealing is used at a high temperature, the post-annealing process promotes the coalescence of the AlN columnar structure and eliminates the dislocations inside the AlN film, which can greatly improve the sputtering on sapphire substrates. The crystal quality of the AlN film [13]. After the high-temperature annealing treatment, the columnar structure of the AlN surface contains some impurities, i.e., oxygen-containing compounds and nitrogen oxide compounds, after condensation [14, 15, 16, 17]. The surface morphology of the film can be further improved by using some homoepitaxial methods to ensure that the AlN epitaxial layer has a uniform step structure and a lower RMS roughness [18]. However, AlN homogeneous epitaxy requires high-temperature equipment exceeding 1250°C, which is expensive. Therefore, we studied the use of commercial MOCVD equipment to directly grow AlGaN layers on two templates before and after annealing.

In this study, the strain evolution state of high-temperature annealing and the low-temperature regrowth process was studied by comparing the high-temperature annealing and non-high-temperature annealing of sputtered AlN templates with the same thickness. Then, high Al composition AlGaN was grown on these templates. Through high-resolution XRD (HRXRD) and atomic force microscopy (AFM), the crystal quality, surface morphology, and stress mode of the regrown high-Al composition AlGaN thin films on the two templates were studied.

Experimental Methods

Part of the high-temperature annealing experiment was completed at Ultratrend Technologies Inc in Hangzhou Zhejiang. A 200-nm-thick AlN film was sputter-grown on three c-plane sapphire substrates. The RF magnetron reactive sputtering method was used with the following conditions: The reaction atmosphere was high-purity nitrogen, the distance between the substrate and the target was 6 cm, the substrate temperature was maintained at 620 °C, and the RF power was 715 W. After that, two sputtered AlN epitaxial wafers were bonded ”face-to-face”, and at 1680 °C, and Ar and N_2 were mixed for high-temperature annealing for 3 h. The purpose of face-to-face bonding is to prevent the thermal decomposition of the AlN film during high-temperature annealing. After the high-temperature annealing was completed, it was quickly cooled to room temperature within 0.5 h.

Next, the growth of the upper layer AlGaN thin film with a high Al composition was completed at Jiangsu Ginjoy Semiconductor Co., Ltd., using MOCVD (Veeco K465i MOCVD system). Because the limit temperature of the equipment can only reach 1100 °C, the ideal temperature for homogeneous epitaxial AlN growth could not be reached. Thus, we adopted a new method for epitaxial AlGaN growth directly onto the AlN template under relatively low temperature conditions and obtained relatively good results. Two sets of epitaxial wafers were placed at the same time on one end of the same circle of the graphite disk to keep the growth environment completely consistent. Trimethylgallium (TMG) and trimethylaluminum (TMA) were used as class III precursor materials, and NH_3 was used as a nitrogen precursor. In the H_2 and NH_3 atmospheres, the impurities on the AlN surface were removed. The columnar crystals on the surface after annealing contained many impurities. Under an NH_3 atmosphere, these columnar crystals can be removed as oxides or nitrogen oxides containing Al [19]. Afterwards, the growth of the AlGaN transition layer and the AlGaN epitaxial layer composed of AlGaN was completed at 1080 °C.

Results and Discussion

We estimated the dislocation density of the SP-AlN template, HTA-AlN template and regrown AlGaN layer based on the test results in Fig.1. In-plane diffraction measurement for characterizing the (10-10) XRC-FWHM value is difficult. Therefore, (10-10) XRC-FWHM is calculated with (0002) XRC-FWHM and (10-12) XRC-FWHM. Usually, the (0002) plane and (10-12) rocking curves (RCs) of AlGaN materials are used, and the half-peak width of the rocking curves of the symmetric and asymmetric planes is used to estimate the dislocation density of the material. There are currently several formulas that are used for estimating the dislocation density, of which the most commonly used are the following [20]:

$$\begin{aligned} \rho_{\text{screw}} &= \frac{\beta^2_{(0002)}}{2\pi \ln 2 \times \left|\vec{b}_c^2\right|} \\ \rho_{\text{edge}} &= \frac{\beta^2_{(10\text{-}12)}}{2\pi \ln 2 \times \left|\vec{b}_a^2\right|} \end{aligned} \quad (1)$$

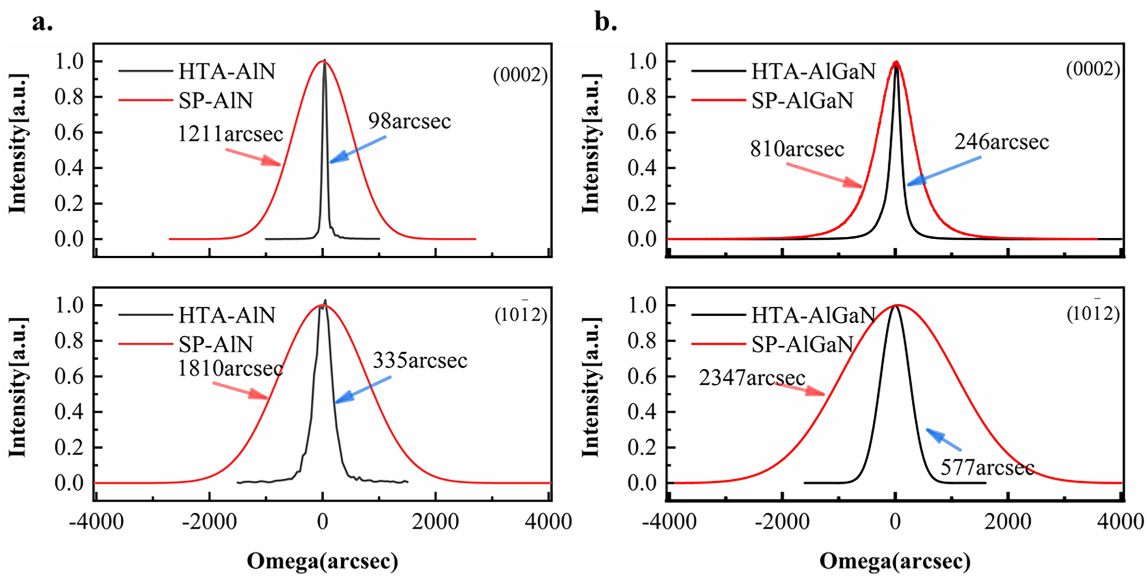

Fig. 1: XRD test of the AlGaN crystal quality.(a) Two AlN template rocking curves; (b) Two template AlGaN rocking curves after regrowth is completed.

Among them, the six parameter distributions of ρscrew, ρedge, $\beta_{(0002)}$,$\beta_{(10\text{-}12)}$, $\vec{b}_a$ and $\vec{b}_c$ are the screw dislocation density, edge dislocation density, (0002) plane RC scan half width, (10-12) half-peak width of the plane RC scan, Burgers vector in c-plane and vertical c-plane Burgers vector, respectively.Usually, in-plane diffraction measurement for characterizing the (10-10) XRC-FWHM value is difficult. Therefore, (10-10) XRC-FWHM is calculated with (0002) XRC-FWHM and (10-12) XRC-FWHM. In the calculation of the dislocation density of AlGaN materials, the lattice constant a is often used in place of the Burgers vector in the c-plane, and the lattice constant c is used in place of the Burgers vector in the vertical c-plane.

Table 1: Dislocation density of the epitaxial layers of two templates.

	RC FWHM		Dislocation density	
Sample	(0002)	(10-12)	$\rho_{\text{screw}}/\text{cm}^{-2}$	$\rho_{\text{edge}}/\text{cm}^{-2}$
SP-AlN	1211	1810	3.2×10^9	1.8×10^{10}
HTA-AlN	**98**	**335**	2.1×10^7	6.8×10^8
SP-AlGaN	810	2347	1.3×10^9	3.0×10^{10}
HTA-AlGaN	**246**	**577**	1.2×10^8	1.8×10^9

Table 1 distincts the calculation results of dislocation density.From the calculation data in the above table, it can be concluded that the AlN template after high-temperature annealing can significantly reduce the dislocation density in the AlN/AlGaN layer by more than an order of magnitude. This finding further proves that high-quality and high-Al components can be grown on a high-temperature annealed AlN template. Feasibility of the AlGaN solution.

Fig. 2.(a)(b) shows the AFM images before and after annealing of the sputtered AlN film. The surface of the SP-AlN template before annealing was covered with columnar structures with a root mean square roughness (RMS) of 2.01 nm, and the surface quality was poor. After high-temperature annealing, the columnar structures coalesced, and the RMS was further reduced to 0.33 nm.

The AFM images after growing AlGaN based on the SP-AlN and HTA-AlN templates are shown in Fig. 2. (c) (d). From this figure, we can see that the surface of AlGaN based on SP-AlN growth contains a certain number of V-shaped pits formed by threading dislocations. The AlGaN grown based on the HTA-AlN template has a more uniform step structure and lower RMS roughness.

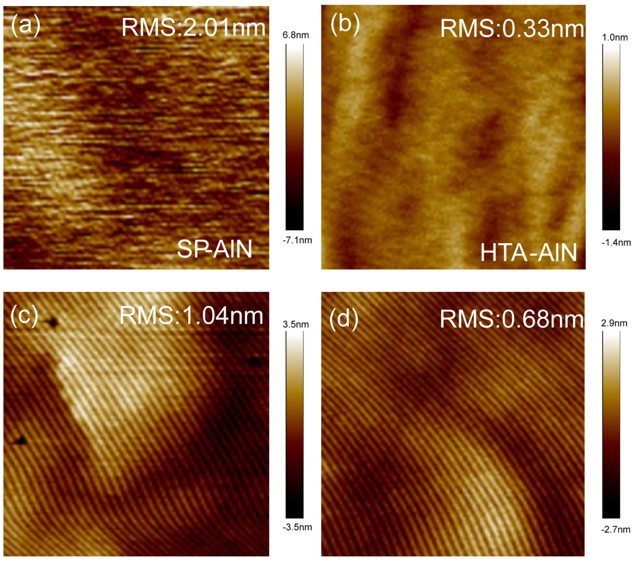

Fig. 2: AFM test $2 \times 2\mu\text{m}^2$ surface topography. (a) Sputtered unannealed AlN; (b) HTA-AlN; (c) Sputtered unannealed AlN directly epitaxial AlGaN; (d) HTA-AlN epitaxial AlGaN.

Fig. 3. shows the XRD test of $2\theta - \omega$ on the (0002) plane of the AlGaN epitaxial layer. First, it should be clear that when AlGaN grows along the c-axis direction, the lattice constant c calculated according to the (0002) plane diffraction angle and Bragg's law is still correct, but the Al composition cannot be directly calculated using Vergard's law. The $2\theta - \omega$ scan of the asymmetric plane is required to determine the lattice constant a. Usually, we measure the (10-12) plane to calculate the lattice constant a. The lattice constants c and a of the hexagonal AlGaN system satisfy the following quantitative relationship:

$$\frac{1}{d_{hkl}^2} = \frac{4\left(h^2 + hk + k^2\right)}{3a^2} + \frac{1}{c^2} \tag{2}$$

According to the above formula, the lattice constant of the AlGaN material can be determined. After obtaining the in-plane lattice constant, the stress on the AlGaN epitaxial film can actually be obtained. Based on the assumption of the nitride biaxial strain, a method of calculating the strain directly using the lattice constant c is used here [21]:

$$\sigma = \frac{2C_{13}^2 - C_{33} \cdot (C_{11} + C_{12})}{2C_{13}} \cdot \frac{c_{film} - c_{bulk}}{c_{bulk}} \tag{3}$$

where σ is the in-plane strain, C_{ij} is the elastic coefficient, and C_{bulk} and C_{film} are the c-axis lattice constants of bulk and thin film materials, respectively. The elasticity coefficient of the AlN material and the c-axis lattice constant under no stress need to be used here. The values of C_{11}, C_{12}, C_{13} and C_{33} are 396 GPa, 137 GPa, 108 GPa and 373 GPa, respectively [22], and the value of cbulk is 0.4982 nm [23]. After the calculation, the stresses in the SP-AlN and HTA-AlN templates before growing the AlGaN layer were 0.4892 GPa and -0.1631 GPa, respectively.

Table 2: Sample lattice constant and strain analysis.

Sample	Diffraction maximum	Lattice constant
	(deg)	(Å)
SP-AlN	18.0244	4.979
HTA-AlN	18.0061	4.983

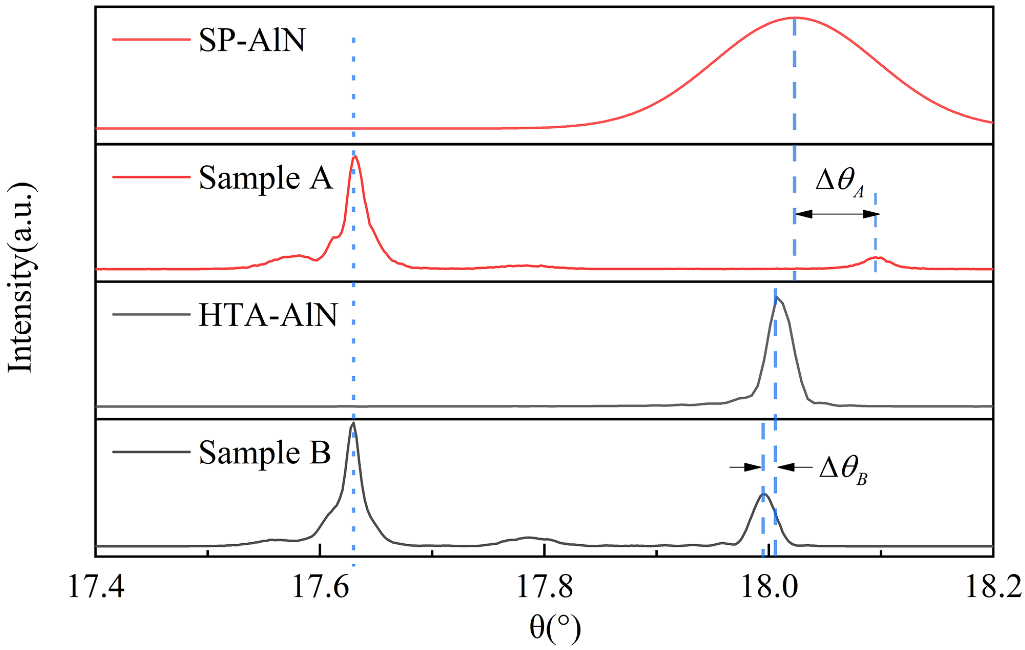

Fig. 3: XRD test of $2\theta - \omega$ of the AlGaN epitaxial layer.

Lattice constant and strain analysis results obvious that HTA-AlN after high temperature treatment are in the state of in-plane compressive strain. The compressive strain in HTA-AlN was released to a certain extent.

The position of the XRD peak reflects the size of the lattice constant of the thin film. For binary compounds, such as GaN and AlN, the change in the peak position in the strain state depends only on the magnitude of the stress it is subjected to. For the ternary alloy AlGaN, the change in the peak position is affected by the changes in the Al composition and stress. It is difficult for XRD to completely distinguish the effect of the Al composition and stress on the change in peak position. In this study, we indirectly studied the stress changes in the two AlGaN thin films through the change in the AlN peak position. It can be seen from Fig. 3 that $\Delta\theta_A > 0$ and $\Delta\theta_B < 0$. This finding indicates that the SP-AlN film is also subjected to tensile stress from the AlGaN film.

Regarding the source of the tensile stress in this part, we believe that it is related to the growth mode of the AlGaN material with a high Al composition. Due to the high surface migration barrier of Al atoms, it is difficult for the atoms to reach the optimal lattice point during growth and form a two-step flow growth mode, so the growth is basically based on three-dimensional island growth. The 3D islands on the surface of AlGaN with high Al composition produced a large amount of tensile stress during the merging process.

Based on the above experimental results and existing research results, we have summarized the growth model based on the HTA-AlN/sapphire template for the high-temperature growth of high AlN mole fraction AlGaN in Fig. 4. The high-temperature annealed sputtered AlN template, due to the low density of the screw and mixed thread dislocations on the surface, will produce sporadic hillock structure growth.[24]. When grown on sputtered AlN without annealing, three-dimensional growth is implemented to reduce the large tensile stress. When grown directly on the HTA-AlN layer, the strain in AlN is further released after high-temperature annealing. The sporadic hillock structure at the growth interface increases the roughness of the interface. From the beginning of AlGaN growth, three-dimensional growth begins. Dislocations will bend during three-dimensional growth. In thick AlGaN growth, AlGaN grows two-dimensionally and has a relatively flat surface shape. Therefore, AlGaN based on HTA-AlN can be directly grown at high temperature, and the high AlN mole fraction can still obtain good crystal orientation and surface conditions.

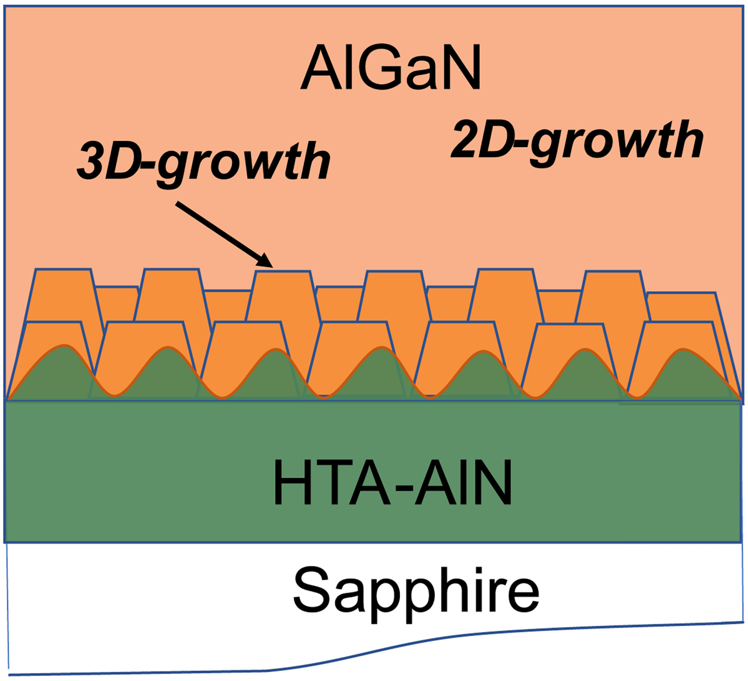

Fig. 4: The principle of low-temperature growth of AlGaN on HTA-AlN.

Conclusions

In this article, we used a high-temperature annealing process to prepare high-quality AlN thin films with a surface roughness (RMS) of only 0.33 nm. Through the high-temperature annealing process, the dislocation density in SP-AlN is reduced by two orders of magnitude.At relatively low temperatures, high-quality epitaxy of the AlGaN material is achieved without using the AlN homoepitaxial layer. AlGaN materials based on high-temperature annealing AlN templates grown at low temperature have a wide range of application markets.

References

[1] Asif Khan, Krishnan Balakrishnan, and Tom Katona. Ultraviolet light-emitting diodes based on group three nitrides. *Nature Photonics*, 2(2):77–84, 2008.

[2] H. Kim, K. K. Choi, K. K. Kim, J. Cho, S. N. Lee, Y. Park, J. S. Kwak, and T. Y. Seong. Light-extraction enhancement of vertical-injection gan-based light-emitting diodes fabricated with highly integrated surface textures. *Optics Letters*, 33(11):1273–5, 2008.

[3] Hideki Hirayama, Noritoshi Maeda, Sachie Fujikawa, Shiro Toyoda, and Norihiko Kamata. Recent progress and future prospects of algan-based high-efficiency deep-ultraviolet light-emitting diodes. *Jpn.j.appl.phys*, 53(10):100209, 2014.

[4] Yoshitaka Taniyasu, Makoto Kasu, and Toshiki Makimoto. An aluminium nitride light-emitting diode with a wavelength of 210?nanometres. *Nature*, 441(7091):325–328, 2006.

[5] Mrs Bulletin. Advances in bulk crystal growth of aln and gan. *Mrs Bulletin*, 34, 2009.

[6] 282-nm algan-based deep ultraviolet light-emitting diodes with improved performance on nano-patterned saoohire substrates. *Applied Physics Letters*, 102(24):241113.1–241113.4, 2013.

[7] S. C. Jain, M. Willander, J. Narayan, and R. Van Overstraeten. Iii–nitrides: Growth, characterization, and properties. *Journal of Applied Physics*, 87(3):965–1006, 2000.

[8] N. Teraguchi, A. Suzuki, Y. Saito, T. Yamaguchi, and Y. Nanishi. Growth of aln films on sic substrates by rf-mbe and rf-mee. *Journal of Crystal Growth*, 230(3):392–397, 2001.

[9] Lisheng Zhang, Fujun Xu, Jiaming Wang, Chenguang He, Weiwei Guo, Mingxing Wang, Bowen Sheng, Lin Lu, Zhixin Qin, and Xinqiang Wang. High-quality aln epitaxy on nano-patterned sapphire substrates prepared by nano-imprint lithography. *Scientific Reports*, 6:35934, 2016.

[10] R. Jain, W. Sun, J. Yang, M. Shatalov, X. Hu, A. Sattu, A. Lunev, J. Deng, I. Shturm, and Y. Bilenko. Migration enhanced lateral epitaxial overgrowth of ain and aigan for high reliability deep ultraviolet light emitting diodes. *Applied Physics Letters*, 93(5):37–39, 2008.

[11] Kazuhito Ban, Jun Ichi Yamamoto, Kenichiro Takeda, Kimiyasu Ide, and Hiroshi Amano. Internal quantum efficiency of whole-composition-range algan multiquantum wells. *Applied Physics Express*, 4(5):2101, 2011.

[12] Myunghee Kim, Jitsuo Ohta, Atsushi Kobayashi, Hiroshi Fujioka, and Masaharu Oshima. Epitaxial growth mechanisms of aln on sic substrates at room temperature. *Applied Physics Letters*, 91(15):p.151903.1–151903.3, 2007.

[13] Hideto Miyake, Chia Hung Lin, Kenta Tokoro, and Kazumasa Hiramatsu. Preparation of high-quality aln on sapphire by high-temperature face-to-face annealing. *Journal of Crystal Growth*, 456:155–159, 2016.

[14] M. X. Wang, F. J. Xu, N. Xie, Y. H. Sun, B. Y. Liu, W. K. Ge, X. N. Kang, Z. X. Qin, X. L. Yang, and X. Q. and Wang. High-temperature annealing induced evolution of strain in aln epitaxial films grown on sapphire substrates. *Applied Physics Letters*, 114(11), 2019.

[15] Hideto Miyake, Chia Hung Lin, Kenta Tokoro, and Kazumasa Hiramatsu. Preparation of high-quality aln on sapphire by high-temperature face-to-face annealing. *Journal of Crystal Growth*, 456:155–159, 2016.

[16] Xiao Shiyu, Suzuki Ryoya, Miyake Hideto, Harada Shunta, and Ujihara Toru. Improvement mechanism of sputtered aln films by high-temperature annealing. *Journal of Crystal Growth*, pages S0022024818304214–, 2018.

[17] Kenjiro Uesugi, Kanako Shojiki, Yuta Tezen, Yusuke Hayashi, and Hideto Miyake. Suppression of dislocation-induced spiral hillocks in movpe-grown algan on face-to-face annealed sputter-deposited aln template. *Applied Physics Letters*, 116(6):062101, 2020.

[18] Duc V Dinh, Hiroshi Amano, and Markus Pristovsek. Movpe growth and high-temperature annealing of (101¯0) aln layers on (101¯0) sapphire. *Journal of Crystal Growth*, 502:14–18, 2018.

[19] Junya Hakamata, Yuta Kawase, Lin Dong, Sho Iwayama, Motoaki Iwaya, Tetsuya Takeuchi, Satoshi Kamiyama, Hideto Miyake, and Isamu Akasaki. Growth of high quality aln and algan films on sputtered aln/sapphire templates via high temperature annealing. *Physica Status Solidi B-basic Solid State Physics*, 255(5):1700506, 2018.

[20] S R Lee, A West, A A Allerman, K E Waldrip, D M Follstaedt, P P Provencio, D D Koleske, and C R Abernathy. Effect of threading dislocations on the bragg peakwidths of gan, algan, and aln heterolayers. *Applied Physics Letters*, 86(24):241904, 2005.

[21] R Cebulla, R Wendt, and K Ellmer. Al-doped zinc oxide films deposited by simultaneous rf and dc excitation of a magnetron plasma: Relationships between plasma parameters and structural and electrical film properties. *Journal of Applied Physics*, 83(2):1087–1095, 1998.

[22] A F Wright. Elastic properties of zinc-blende and wurtzite aln, gan, and inn. *Journal of Applied Physics*, 82(6):2833–2839, 1997.

[23] Shiro Kobayashi and Klaus Müllen. Encyclopedia of polymeric nanomaterials ||. 10.1007/978-3-642-29648-2, 2015.

[24] Kenjiro Uesugi, Kanako Shojiki, Yuta Tezen, Yusuke Hayashi, and Hideto Miyake. Suppression of dislocation-induced spiral hillocks in movpe-grown algan on face-to-face annealed sputter-deposited aln template. *Applied Physics Letters*, 116(6):062101, 2020.